Record Open-Circuit Voltages >1.26 V in Planar Methylammonium Lead Iodide Solar Cells by Suppressing Interfacial Recombination

Zhifa Liu[1,2†], Lisa Krückemeier[1†*], Benedikt Krogmeier[1], Benjamin Klingebiel[1], José A. Márquez[3], Sergiu Levcenko[3], Senol Öz[4], Sanjay Mathur[4], Uwe Rau[1], Thomas Unold[3], and Thomas Kirchartz[1,5*]

[1]IEK5-Photovoltaics, Forschungszentrum Jülich, 52425 Jülich, Germany

[2]State Key Laboratory of Structural Chemistry, Fujian Institute of Research on the Structure of Matter, Chinese Academy of Sciences, Fuzhou, Fujian 350002, P. R. China

[3]Department of Structure and Dynamics of Energy Materials, Helmholtz-Zentrum-Berlin, Hahn-Meitner-Platz 1, D-14109 Berlin, Germany

[4] Institute of Inorganic Chemistry, University of Cologne, Greinstr. 6, 50939, Cologne, Germany

[5]Faculty of Engineering and CENIDE, University of Duisburg-Essen, Carl-Benz-Str. 199, 47057 Duisburg, Germany

[†]equal contribution, *t.kirchartz@fz-juelich.de, *l.krueckemeier@fz-juelich.de

Abstract

We demonstrate open-circuit voltages exceeding 1.26 V for $CH_3NH_3PbI_3$ solar cells by careful process optimization of the perovskite and its interfaces to the electron and hole transport layers. This open-circuit voltage is the highest reported so far in a full MAPI cell stack and only 64 mV below the maximum open circuit voltage that is possible for this material. We confirm these values for the open circuit voltage by independent measurements of the external photoluminescence quantum efficiency reaching values of 5 % for the fully processed solar cell. We further find exceptionally long photoluminescence lifetimes in full cells and in layer stacks involving one or two contact layers. Numerical simulations reveal that these long photoluminescence lifetimes are only possible with extremely low interface recombination velocities between absorber and contact materials.

For mature photovoltaic technologies the biggest challenge when improving their power conversion efficiencies is approaching the radiative limit of the open-circuit voltage by minimizing non-radiative recombination processes in the bulk, at surfaces and at contact layers.[1-2] This statement also holds for the rapidly developing class of lead-halide perovskite solar cells. From the beginning of their development this type of solar cells has demonstrated astonishingly high open-circuit voltages in relation to their band gap energy. Already the first paper on $CH_3NH_3PbI_3$ (MAPI) based solar cells with > 10% efficiency[3], showed an open-circuit voltage $V_{oc} \approx 1.1$ V. Nowadays, photovoltaic power conversion efficiencies of MAPI have risen above 23 %[4] and open-circuit voltages of perovskites with band gaps $E_g \approx 1.6$ eV are now approaching or sometimes exceeding 1.2 V (with the radiative limit for the V_{oc} in MAPI being ~1.32 V[5-8]). It has recently been shown that a quasi-Fermi level splitting corresponding to an internal open circuit voltage of 1.28 V is possible in MAPI films on glass proving that the bulk material has the potential to come within 40 to 50 mV of its thermodynamic limit.[9] However, the presence of contacts has so far limited the open-circuit voltage V_{oc} achievable in a completed device. The lowest values of V_{oc}-loss relative to the radiative limit correspond to the highest values of external luminescence quantum efficiency ($Q_{e,lum}$) at injection conditions corresponding to one sun.[10-11] Saliba et al.[12] showed record values for $Q_{e,lum}$ ~1 % corresponding to voltage losses of about $kT/q\ln(100) = 120$ mV in Rb-containing perovskites with a band gap slightly above 1.6 eV. Any progress beyond this value towards lower non-radiative recombination losses requires careful control of all non-radiative recombination pathways, in the bulk and at the interfaces towards the electron and hole extracting layers.

Here, we prepare and characterize MAPI solar cells that include 10 mol% $PbCl_2$ of the total Pb during fabrication but incorporate no other cations or anions in the crystal lattice. We use the organic charge extraction layers Poly(triaryl amine) (PTAA) for the hole extraction and [6,6]-phenyl-C_{61}-butyric acid methyl ester (PCBM) for the electron extraction and show how a

variety of small processing improvements allows us to suppress recombination at interfaces and in the bulk substantially to achieve open-circuit voltages around 1.26 V. This results substantially outperforms the open circuit voltages previously reported for other halide perovskites with similar band gaps and approaches the levels previously shown to be only possible in films on glass[9] that were lacking charge extracting contacts. We use steady state photoluminescence (PL) spectroscopy to connect the properties of full solar cells to the ones of films with different contacts as introduced by Sarritzu et al.[13]. Furthermore we combine the steady-state PL with transient photoluminescence (tr-PL) of different layer stacks to correlate the kinetics of the decay with the absolute intensity of the luminescence.

Figure 1a shows a schematic of the full solar cell stack as used in this study, featuring ITO (150 nm) as the transparent conductive oxide, PTAA (~30 nm) as the hole conductor, MAPI (~280nm) as the absorber, PCBM (~45 nm) as the electron transport material as well as BCP (~8 nm) and Ag (80 nm) finishing up the cathode.

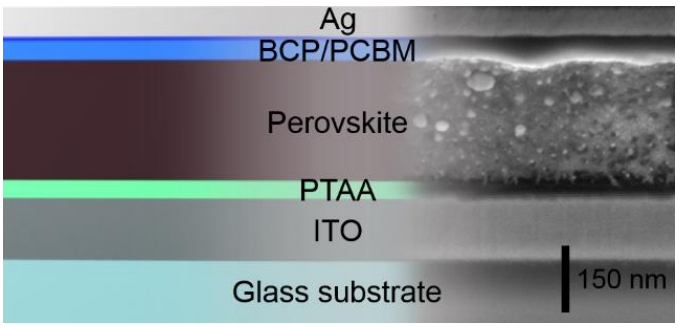

Figure 1: Schematic drawing of the layer stack used in this study combined with a SEM cross section of a solar cell.[14]

In this study we aimed at optimizing simple MAPI layers grown on PTAA for highest possible open-circuit voltage. The process to deposit the MAPI layers by spin coating involved a solution of $Pb(Ac)_2$ (0.54 M), $PbCl_2$ (0.06 M) and MAI (1.8 M) in DMF combined with a very short annealing time of 2 min at 75 °C. Lead acetate based precursors have previously been shown to yield smooth[15] high quality pinhole-free layers[16] and were therefore chosen to achieve highest open-circuit voltages.

Since high open circuit voltages require well passivated surfaces, the optimization also had to include the right choice of processing conditions for PCBM. There are various degrees of freedom in processing the PCBM layer that we can use to optimize the MAPI/PCBM interface for lowest possible recombination rates. These degrees of freedom are - apart from spin-coating parameters itself - the choice of solvent, the post deposition annealing treatment and the atmosphere during spin-coating and subsequent annealing. As shown in ref.[17] higher boiling point solvents can lead to more ordered layers, because the solvent has more time to evaporate than for lower boiling point solvents. In addition, by annealing or by solvent annealing, layer crystallization can be accelerated or slowed down. As part of device optimization, we tested chlorobenzene (CB) and 1,2-dichlorobenzene (1,2-DCB) as solvents for PCBM. Using CB which has a lower boiling point (130 °C) results in a less ordered PCBM layer than in the case of 1,2-DCB having a higher boiling point (180.5 °C). Unlike reported by Shao et al.[18], we found that less ordered PCBM films deposited on our PTAA/MAPI stack lead to substantially higher open-circuit voltages. During our studies we also noted that the ideal processing conditions for the PCBM did vary depending on the choice of hole transport material and depending on the MAPI processing conditions. If we use 1,2-DCB as solvent for PCBM, substantial losses in V_{oc} occur and only open-circuit voltage less than 1.2 V are achievable, revealing how sensitive the process window is to achieve these high open circuit voltages. The opposite trend of V_{oc} with PCBM processing conditions is observed when choosing another HTL layer (PEDOT:PSS) on which the perovskite crystallizes differently (see Supplementary Information (SI), Fig. S1). We therefore assume that the ideal process parameters must always be considered holistically and have to be individually adjusted to each other in order to achieve the best possible results. The process leading to the highest open circuit voltages on PTAA is therefore described in detail in the method section.

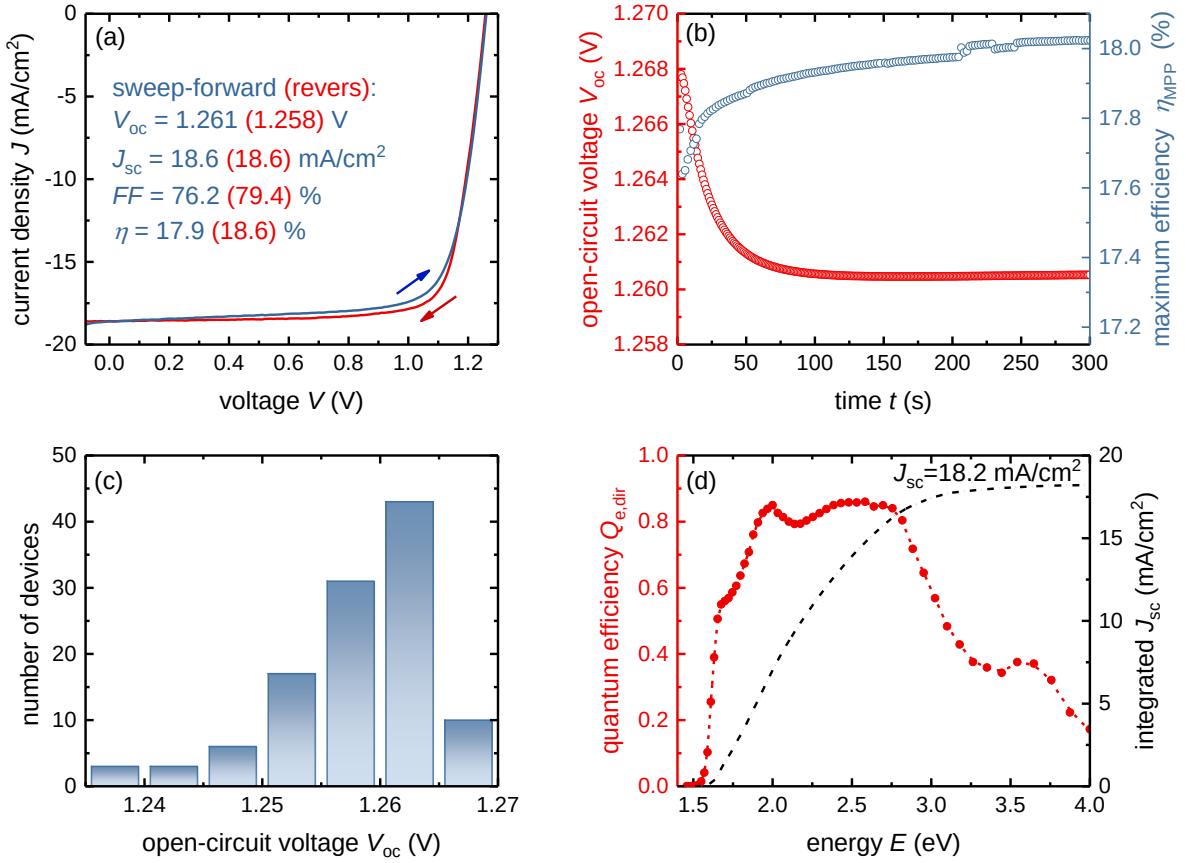

Figure 2: (a) Current density *J* as a function of voltage *V* taken at 100 mV/s scan speed measured under a class AAA solar simulator for a representative MAPI solar cell in this study. (b) Open-circuit voltage V_{oc} and efficiency η tracking for 300 s measured with a white LED resulting in a stabilized value >1.26 V and around 18 %. (c) Histogram of the open-circuit voltage for the number of devices in this study. (d) Quantum efficiency $Q_{e,dir}$ as a function of photon energy *E* with the accumulated short-circuit current density J_{sc} of the cell.

Figure 2a shows the current density-voltage (*JV*) curve of a typical device recorded at a scan speed of 100 mV/s under a class AAA solar simulator under forward and reverse scan conditions. The efficiency is around 18 % but the most remarkable feature is the high open-circuit voltage V_{oc} of ~1.26 V. Figure 2b shows the open-circuit voltage as well as the efficiency measured as a function of time under white light provided by a white LED adjusted to one sun conditions (see SI Fig. S4) confirming that the open-circuit voltage stabilizes above 1.26 V at an efficiency of ~ 18 %. Furthermore, as illustrated by the histogram in Fig. 2c, this high V_{oc} value is reproducible for a series of different devices. In order to reach these high open-circuit voltages, the cell has to be photoactivated either by measuring several current voltage curves

for ~10 mins or by being kept under open-circuit condition by the white light LED (Fig. S4). There have been various reasons proposed to explain the improvement of electronic properties by light soaking such as defect passivation by redistribution of halide ions,[19-20] lattice expansion reducing local strain in the crystal[21] and doping of the fullerene based electron contact layers.[22] Here, we do not aim at further elucidating the mechanisms for light induced improvements in performance, but we note that while we observe improvements in V_{oc} similar to the ones presented by Tsai et al.[21], we do not observe any changes in band gap (based on photoluminescence data shown in Fig. S7) that were suggested to be a result of photoinduced lattice expansion.[21] In contrast, the observations of defect passivation and fullerene doping reported e.g. in refs.[19-20, 22] are completely compatible with our results of improved fill factor and V_{oc} after light soaking.

Figure 2d shows the photovoltaic quantum efficiency $Q_{e,dir}$ of the same solar cell as a function of photon energy E providing further evidence for the measured short-circuit current density. The absorber thickness is around 280 nm implying that the quantum efficiency at the band gap is not perfectly sharp due to the kink in the absorption coefficient of MAPI. Higher thicknesses however typically lead to slightly reduced open-circuit voltages because of the larger volume available for recombination.[23-25] Thus, in order to explore the limits to V_{oc}, we intentionally focused on optimizing the process conditions for fairly thin cells that are not optimized for maximum short-circuit current densities.

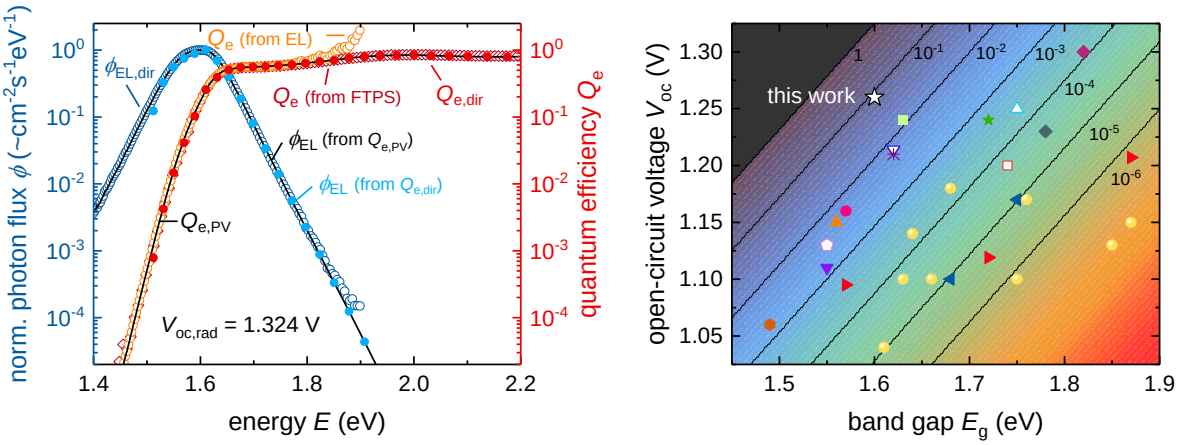

Figure 3: (a) Electroluminescence spectrum $\phi_{EL,dir}$ and quantum efficiency $Q_{e,dir}$ from (EQE and FTPS) of the same cell measured to determine the radiative open-circuit voltage $V_{oc,rad}$ by using the optoelectronic reciprocity relation. The calculation gives a thermodynamic limit for the open-circuit voltage of 1.324 V for the respective device stack. (b) Overview of the open-circuit voltage of lead halide perovskite solar cells as a function of bandgap energy E_g, comparing current state in literature to the V_{oc} in this work. This comparison demonstrates the outstanding record value we have achieved by device optimization. The surface plot illustrates the radiative limit for different external quantum efficiencies (1-10^{-6}) calculated with a step-function like absorptance.

Based on the quantum efficiency shown in Fig. 2d, we may calculate the thermodynamic limit for the open-circuit voltage. Figure 3a shows the electroluminescence spectrum $\phi_{EL,dir}$ of the cell as well as the photovoltaic quantum efficiency $Q_{e,dir}$ on a logarithmic scale. Using the optoelectronic reciprocity theorem,[11] we calculate the solar cell quantum efficiency for the low energy range from the electroluminescence spectrum $\phi_{EL,dir}$ and combined it with $Q_{e,dir}$ to an overall $Q_{e,PV}$, which then is used to determine the radiative saturation-current density

$$J_{0,rad} = q\int_0^\infty Q_{e,PV}(E)\phi_{bb}(E)dE \,. \qquad (1)$$

where q is the elementary charge,

$$\phi_{bb}(E) = \frac{2\pi E^2}{h^3c^2}\frac{1}{\left[\exp\left(E/kT\right)-1\right]} \approx \frac{2\pi E^2}{h^3c^2}\exp\left(\frac{-E}{kT}\right). \qquad (2)$$

is the black body spectrum at temperature T (of the solar cell), h is Planck's constant and c is the speed of light in vacuum. From $J_{0,\mathrm{rad}}$, we may calculate the open-circuit voltage $V_{\mathrm{oc,rad}}$ in the limit that there is only radiative recombination via

$$V_{\mathrm{oc,rad}} = \frac{kT}{q}\ln\left(\frac{J_{\mathrm{sc}}}{J_{0,\mathrm{rad}}}+1\right). \tag{3}$$

Using the values J_{sc} = 18.18 mA/cm^2 and $J_{0,\mathrm{rad}}$ = 9.498·10^{-22} mA/cm^2 as calculated from Eq. (1), we obtain a radiative open-circuit voltage $V_{\mathrm{oc,rad}}$ = 1.324 V, i.e. similar to the values that have been obtained for MAPI in refs.[5-6, 8]. If we compare this radiative open-circuit voltage with the actual open-circuit voltages obtained in this study, we estimate the luminescence quantum efficiency $Q_{\mathrm{e,lum}}$ as a measure of the non-radiative loss using the theory developed originally by Ross[10] and refined and used by many others.[11, 26-28] We obtain from

$$qV_{\mathrm{oc,rad}} - qV_{\mathrm{oc}} = q\Delta V_{\mathrm{oc,nr}} = -kT\ln\left(Q_{\mathrm{e,lum}}\right), \tag{4}$$

a value of 64 mV for the voltage loss $\Delta V_{\mathrm{oc,nr}}$ due to non-radiative recombination. This voltage loss corresponds to an external luminescence quantum efficiency $Q_{\mathrm{e,lum}} = 8.4\%$. This external luminescence quantum efficiency while not being measured directly, is substantially higher than the highest one reported so far, which was ~1% at one sun conditions.[12] Figure 3b shows a comparison between measured values of the open-circuit voltage of lead-halide perovskite solar cells as a function of band gap E_{g} and the Shockley-Queisser (SQ) limit for V_{oc}. The SQ and radiative limit for different external quantum efficiencies is calculated for simplicity with a step-function like absorptance as opposed to the measured photovoltaic quantum efficiency used for Fig. 3a. While the datapoints used for Fig. 3b are certainly a non-exhaustive representation of the literature, we took care to include the results which reported particularly high open-circuit voltages relative to their band gaps (for additional information in Fig. S11 and Tab.SII). Figure 3b shows that so far only one datapoint in the literature has reached a V_{oc} that corresponds to ~1 % external luminescence quantum efficiency. The present work shows

that this level can be substantially overcome in working devices of pure MAPI (with $PbCl_2$ being used during fabrication) without the inclusion of molecules and elements such as K,[29] Rb,[12] or Cs[30] that have previously been used to achieve the highest open-circuit voltages.

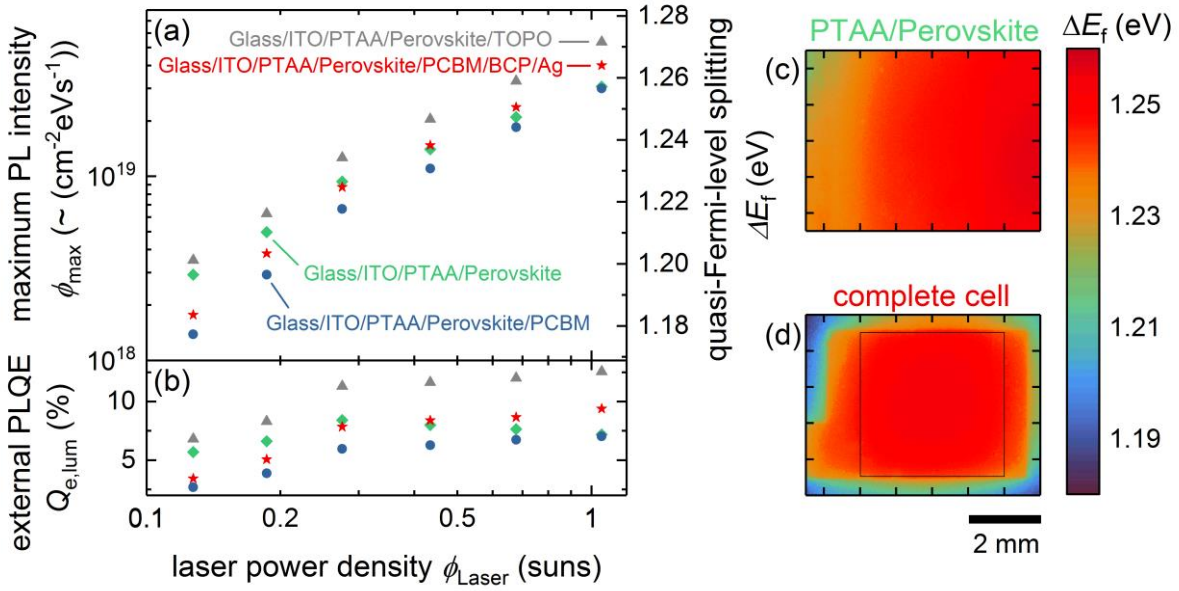

Figure 4: (a) Steady state PL measurements on different interlayer stacks as a function of laser excitation, converted into the quasi-Fermi-level splitting ΔE_f and the external PLQE $Q_{e,lum}$. (b) PL-image of the perovskite layer on PTAA and (c) PL image of the complete cell. The data points in (a) were measured in Jülich and the images in (b) and (c) were measured in Berlin to provide independent confirmation.

As has recently been shown by Stolterfoht et al.[31] in a similar device stack, interface recombination between the perovskite absorber layer and the electron and hole transport layers PCBM and PTAA is a critical factor in achieving the highest possible open-circuit voltages. In order to study interface recombination, we use steady state and transient photoluminescence on completed cells and on different layer stacks with only one contact layer (PTAA) or with both contact layers (PTAA and PCBM) but without metal back contact. We additionally show the PL of a MAPI layer grown on PTAA passivated with the molecule TOPO allowing us to evaluate the quality of the perovskite itself as well as its interface to PTAA and the uncovered surface. Figure 4a shows the steady state photoluminescence as a function of laser fluence used for sample excitation for the four investigated stacks (passivated perovskite, hole contact only,

both contacts, full cell). We show the data for samples that were exposed to light soaking before the measurement. The left y-axis is proportional to the photoluminescence counts but is already expressed as an external luminescence quantum efficiency as discussed in the methods section in the SI. The right y-axis shows the quasi-Fermi level splitting that corresponds to the luminescence quantum efficiency on the left y-axis. The quasi-Fermi level splitting ΔE_f of the solar cell at one sun corresponds to the V_{oc} of the cell and all other quasi-Fermi level splittings are calculated from

$$\Delta E_f = qV_{oc}(\phi_{sun}) + kT \ln\left(\frac{\phi_{PL}}{\phi_{PL,cell}(\phi_{sun})}\right), \quad (5)$$

assuming flat quasi-Fermi levels where $\phi_{PL,cell}$ is the photoluminescence intensity of the solar cell and ϕ_{PL} is the photoluminescence intensity of any of the four types of samples. Thus, any difference in PL intensity of a factor of 10 relative to the PL intensity of the solar cell at an excitation corresponding to one sun would correspond to $kT\ln(10) \approx 60$ meV change in the quasi-Fermi level splitting. We find that the TOPO-passivated sample (grey) has the highest quantum efficiency and a Fermi-energy splitting of ~1.27 eV at 1 sun, which is comparable to the 1.28 eV one previously reported by Braly et al.[9]. However, as an electrically insulating interface minimizing recombination, TOPO does not meet the key requirement for a functional solar cell with reasonably low resistive losses. However, using TOPO as a passivation experiment, it is demonstrated that our bulk material can be prepared in such a way that non-radiative recombination is already very low. When comparing the passivated sample to the other samples, it stands out that the quasi-Fermi-level splitting in the solar cell (red) and in the other layer stacks is only about 10 to 20 meV smaller. This very small difference demonstrates how well our interlayers are adapted and that there are only small non-radiative losses due to surface recombination. We find that the solar cell actually has a slightly higher quasi-Fermi level splitting then their two respective layer stacks without metal. This apparent superiority of the device relative to the other two samples may at first seem surprising. The presence of contacts

should lead to additional surface recombination relative to the typically well passivated bare surfaces of MAPI.[32] Thus, in previous publications,[13, 29, 31] the addition of contacts always led to reduced luminescence and quasi-Fermi level splitting. This is no longer the case in the MAPI samples presented here at least if the detectable luminescence emitted through the front surface is compared. The reason for this observation may be that photon recycling has to be a strong factor in devices being that close to the radiative limit. Thus, the presence of a back reflector which increases reabsorption of light relative to outcoupling towards the back may increase the concentration of charge carriers in the device as well as the luminescence that can be detected.

We get the same result for the PL images of the layer systems measured on a hyperspectral absolute photoluminescence imaging setup which are shown in Fig. 4b and c. Since this setup is calibrated to provide absolute quantum yields, the data give us an additional and independent confirmation of the high quasi-Fermi level splitting we observe in our samples. Here we obtain an external quantum efficiency of 5% for the cell, which is smaller than the results from Figure 4(a), but still the highest value reported so far for a full lead-halide perovskite cell solar cell device. Deviations could be explained, for example, by aging and degradation during sample storage and transport. The image section shows one solar cell of the four existing on the substrate. In the case of the layer system without ETL and silver a contrast between the areas without and with ITO is visible.

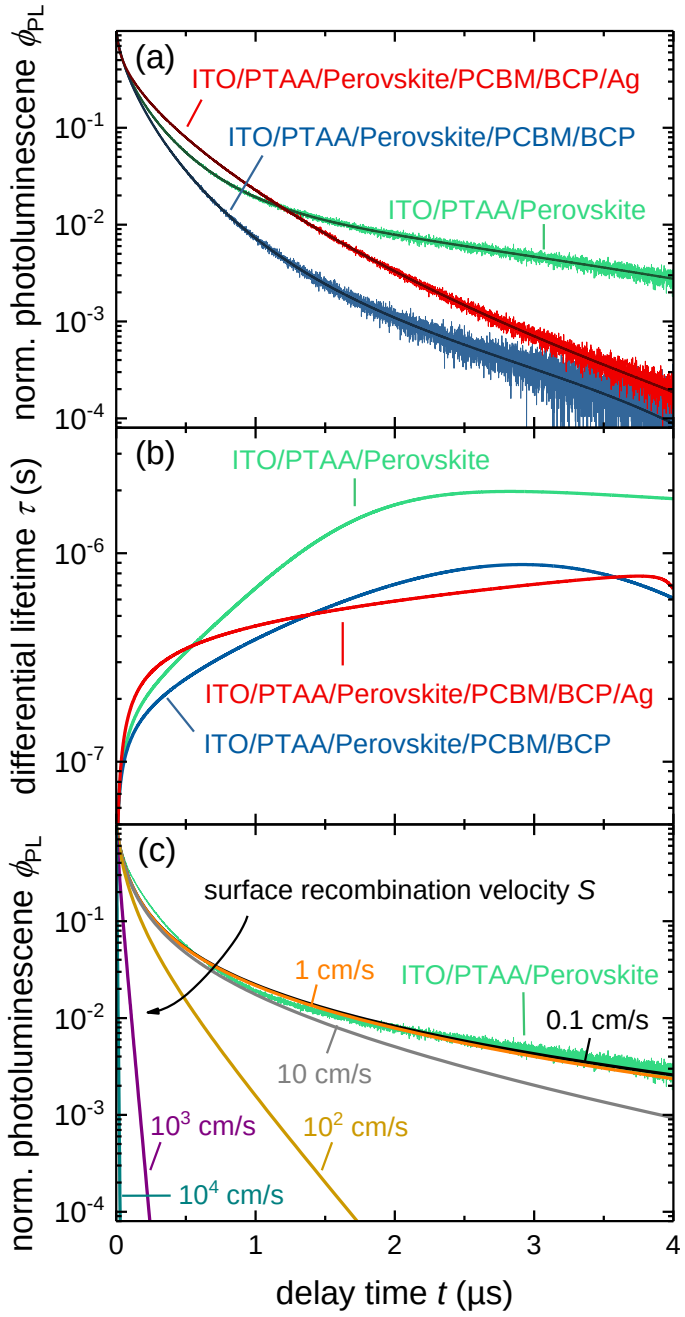

Figure 5: (a) Transient photoluminescence (tr-PL) measurements on different layer stacks, namely the full solar cell (red) and MAPI grown on PTAA without (green) and with PCBM/BCP (blue) as ETL. (b) Differential lifetime τ obtained by taking the derivative of the curves in (a) for every time t. To obtain a smoother derivative, the data in (a) was first fitted (thin lines shown in (a)) and then the derivate was computed from the fitted data according Eq.6. (c) Tr-PL simulations to model the ITO/PTAA/Perovskite stack for different surface velocity S demonstrating that the experimentally measured decay (green) only fits the simulations for very small S.

Contact layers typically quench the luminescence and so should also be clearly visible in transient photoluminescence experiments with the expectation being that the transient becomes

substantially faster in the presence of a contact. In the past, the longer time decay of luminescence of samples with at least one electron or hole accepting layer have been analyzed and interpreted in terms of surface recombination velocities.[31, 33-34] However, in the present case, the contacts did not lead to any substantial quenching of the steady state luminescence. Thus, it is not surprising to see that the transients of the three types of samples shown in Fig. 5a decay quite slowly after a quick initial decay. Figure 5b shows the differential lifetimes that follow from

$$\tau = -\left(\frac{\mathrm{d} \ln\left(\phi_{\mathrm{PL}}\right)}{\mathrm{d}t} \right)^{-1}, \tag{6}$$

The lifetimes increase for longer times and saturate for long times in the low µs range for all three scenarios. The quantitative interpretation of PL transients of layer stacks involving charge extracting contacts is complicated by the multitude of competing mechanisms that have to be taken into account. Here, we therefore performed numerical simulations with the software TCAD Sentaurus as discussed in more detail in ref.[33] to obtain a more quantitative understanding of the surface recombination velocity at the perovskite/PTAA interface. Based on the parameters given in the SI, we performed simulations for different values of the surface recombination velocity that show that these long transients are most compatible with values of $S \sim 1$ cm/s or smaller in which case the shape of the transient is to a large degree determined by the recombination parameters assumed for the bulk material. Thus, the long transients are fully compatible with the absolute luminescence measurements and provide evidence for the extremely low levels of interfacial recombination.

In conclusion, we have shown that by process optimization of the perovskite film and the contact layers, the open-circuit voltage of simple MAPI can be tuned up to 1.26 V without any addition of passivating alkali metals such as Cs, K or Rb. In addition, extremely low surface recombination velocities have been measured and are required in order to rationalize the high open-circuit voltage. While the current study focusses on eliminating and characterizing losses

due to bulk and interface recombination, future improvements in open-circuit voltage will require optimizing the layer stack for minimum parasitic absorption and maximum efficiency of photon recycling[35-37] in a similar way as efficiency optimization in GaAs solar cells has been achieved in the past.[38]

TOC Figure

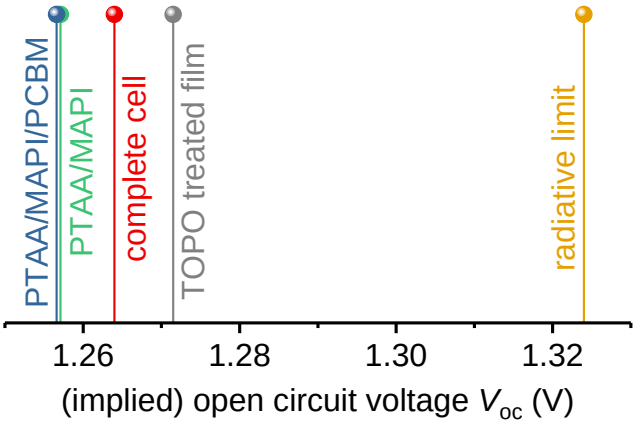

Corresponding Author

*To whom correspondence should be addressed. E-Mail: t.kirchartz@fz-juelich.de, l.krueckemeier@fz-juelich.de

Notes

The authors declare no competing financial interests.

Additional information

Supplementary information is available in the online version of the paper. Reprints and permissions information is available online at [URL will be introduced by the publisher]. Correspondence and requests for data should be addressed to L.K. or T.K.

Acknowledgements

The authors acknowledge support from the Impuls- und Vernetzungsfonds der Helmholtz Gesellschaft via the project PEROSEED. TK and LK thank the Bavarian Ministry of Economic Affairs and Media, Energy and Technology for the joint projects in the framework of the Helmholtz Institute Erlangen-Nürnberg.

……

References

1. Green, M. A., Radiative Efficiency of State-of-the-Art Photovoltaic Cells. *Progress in Photovoltaics* **2012,** *20* (4), 472-476.
2. Rau, U.; Blank, B.; Müller, T. C. M.; Kirchartz, T., Efficiency Potential of Photovoltaic Materials and Devices Unveiled by Detailed-Balance Analysis. *Physical Review Applied* **2017,** *7* (4), 044016.
3. Lee, M. M.; Teuscher, J.; Miyasaka, T.; Murakami, T. N.; Snaith, H. J., Efficient Hybrid Solar Cells Based on Meso-Superstructured Organometal Halide Perovskites. *Science* **2012,** *338* (6107), 643-647.
4. Jeon, N. J.; Na, H.; Jung, E. H.; Yang, T.-Y.; Lee, Y. G.; Kim, G.; Shin, H.-W.; Seok, S. I.; Lee, J.; Seo, J., A Fluorene-Terminated Hole-Transporting Material for Highly Efficient and Stable Perovskite Solar Cells. *Nature Energy* **2018,** *3* (8), 682.
5. Tvingstedt, K.; Malinkiewicz, O.; Baumann, A.; Deibel, C.; Snaith, H. J.; Dyakonov, V.; Bolink, H. J., Radiative Efficiency of Lead Iodide Based Perovskite Solar Cells. *Sci. Rep* **2014,** *4*, 6071.
6. Tress, W.; Marinova, N.; Inganas, O.; Nazeeruddin, M. K.; Zakeeruddin, S. M.; Graetzel, M., Predicting the Open-Circuit Voltage of $Ch_3nh_3pbi_3$ Perovskite Solar Cells Using Electroluminescence and Photovoltaic Quantum Efficiency Spectra: The Role of Radiative and Non-Radiative Recombination. *Advanced Energy Materials* **2015,** *5* (3), 1400812.
7. Correa-Baena, J. P.; Saliba, M.; Buonassisi, T.; Grätzel, M.; Abate, A.; Tress, W.; Hagfeldt, A., Promises and Challenges of Perovskite Solar Cells. *Science* **2017,** *358* (6364), 739.
8. Yao, J. Z.; Kirchartz, T.; Vezie, M. S.; Faist, M. A.; Gong, W.; He, Z. C.; Wu, H. B.; Troughton, J.; Watson, T.; Bryant, D.; Nelson, J., Quantifying Losses in Open-Circuit Voltage in Solution-Processable Solar Cells. *Physical Review Applied* **2015,** *4* (1), 014020.
9. Braly, I. L.; deQuilettes, D. W.; Pazos-Outon, L. M.; Burke, S.; Ziffer, M. E.; Ginger, D. S.; Hillhouse, H. W., Hybrid Perovskite Films Approaching the Radiative Limit with over 90% Photoluminescence Quantum Efficiency. *Nature Photonics* **2018,** *12*, 355-361.

10. Ross, R. T., Some Thermodynamics of Photochemical Systems. *Journal of Chemical Physics* **1967,** *46*, 4590-4593.
11. Rau, U., Reciprocity Relation between Photovoltaic Quantum Efficiency and Electroluminescent Emission of Solar Cells. *Physical Review B* **2007,** *76* (8), 085303.
12. Saliba, M.; Matsui, T.; Domanski, K.; Seo, J. Y.; Ummadisingu, A.; Zakeeruddin, S. M.; Correa-Baena, J. P.; Tress, W. R.; Abate, A.; Hagfeldt, A.; Grätzel, M., Incorporation of Rubidium Cations into Perovskite Solar Cells Improves Photovoltaic Performance. *Science* **2016,** *354* (6309), 206.
13. Sarritzu, V.; Sestu, N.; Marongiu, D.; Chang, X.; Masi, S.; Rizzo, A.; Colella, S.; Quochi, F.; Saba, M.; Mura, A.; Bongiovanni, G., Optical Determination of Shockley-Read-Hall and Interface Recombination Currents in Hybrid Perovskites. *Scientific Reports* **2017,** *7*, 44629.
14. Albrecht, W.; Moers, J.; Hermanns, B., Hnf-Helmholtz Nano Facility. *Journal of large-scale research facilities JLSRF* **2017,** *3*, 112.
15. Zhang, W.; Saliba, M.; Moore, D. T.; Pathak, S. K.; Hörantner, M. T.; Stergiopoulos, T.; Stranks, S. D.; Eperon, G. E.; Alexander-Webber, J. A.; Abate, A., Ultrasmooth Organic–Inorganic Perovskite Thin-Film Formation and Crystallization for Efficient Planar Heterojunction Solar Cells. *Nature communications* **2015,** *6*, 6142.
16. Qiu, W.; Merckx, T.; Jaysankar, M.; de la Huerta, C. M.; Rakocevic, L.; Zhang, W.; Paetzold, U.; Gehlhaar, R.; Froyen, L.; Poortmans, J., Pinhole-Free Perovskite Films for Efficient Solar Modules. *Energy & Environmental Science* **2016,** *9* (2), 484-489.
17. An, T. K.; Park, S. J.; Ahn, E. S.; Jang, S. H.; Kim, Y.; Kim, K.; Cha, H.; Kim, Y. J.; Kim, S. H.; Park, C. E., Solvent Boiling Point Affects the Crystalline Properties and Performances of Anthradithiophene-Based Devices. *Dyes and Pigments* **2015,** *114*, 60-68.
18. Shao, Y.; Yuan, Y.; Huang, J., Correlation of Energy Disorder and Open-Circuit Voltage in Hybrid Perovskite Solar Cells. *Nature Energy* **2016,** *1*, 15001.
19. deQuilettes, D. W.; Zhang, W.; Burlakov, V. M.; Graham, D. J.; Leijtens, T.; Osherov, A.; Bulovic, V.; Snaith, H. J.; Ginger, D. S.; Stranks, S. D., Photo-Induced Halide Redistribution in Organic-Inorganic Perovskite Films. *Nat. Commun* **2016,** *7*, 11683.
20. Mosconi, E.; Meggiolaro, D.; Snaith, H. J.; Stranks, S. D.; De Angelis, F., Light-Induced Annihilation of Frenkel Defects in Organo-Lead Halide Perovskites. *Energy & Environmental Science* **2016,** *9* (10), 3180-3187.
21. Tsai, H.; Asadpour, R.; Blancon, J. C.; Stoumpos, C. C.; Durand, O.; Strzalka, J. W.; Chen, B.; Verduzco, R.; Ajayan, P. M.; Tretiak, S.; Even, J.; Alam, M. A.; Kanatzidis, M. G.; Nie, W.; Mohite, A. D., Light-Induced Lattice Expansion Leads to High-Efficiency Perovskite Solar Cells. *Science* **2018,** *360* (6384), 67.
22. De Bastiani, M.; Dell'Erba, G.; Gandini, M.; D'Innocenzo, V.; Neutzner, S.; Kandada, A. R. S.; Grancini, G.; Binda, M.; Prato, M.; Ball, J. M., Ion Migration and the Role of Preconditioning Cycles in the Stabilization of the J–V Characteristics of Inverted Hybrid Perovskite Solar Cells. *Advanced Energy Materials* **2016,** *6* (2), 1501453.
23. Brendel, R.; Queisser, H. J., On the Thickness Dependence of Open-Circuit Voltages of P-N-Junction Solar-Cells. *Solar Energy Materials and Solar Cells* **1993,** *29* (4), 397-401.
24. Blank, B.; Kirchartz, T.; Lany, S.; Rau, U., Selection Metric for Photovoltaic Materials Screening Based on Detailed-Balance Analysis. *Physical Review Applied* **2017,** *8* (2), 024032.
25. Kirchartz, T.; Rau, U., What Makes a Good Solar Cell? In *Advanced Energy Materials*, Wiley-Blackwell: 2018; Vol. 8, p 1703385.
26. Smestad, G.; Ries, H., Luminescence and Current Voltage Characteristics of Solar-Cells and Optoelectronic Devices. *Solar Energy Materials and Solar Cells* **1992,** *25* (1-2), 51-71.
27. Kirchartz, T.; Nelson, J.; Rau, U., Reciprocity between Charge Injection and Extraction and Its Influence on the Interpretation of Electroluminescence Spectra in Organic Solar Cells. *Physical Review Applied* **2016,** *5* (5), 054003.

28. Vandewal, K.; Tvingstedt, K.; Gadisa, A.; Inganas, O.; Manca, J. V., On the Origin of the Open-Circuit Voltage of Polymer-Fullerene Solar Cells. *Nature Materials* **2009,** *8* (11), 904-909.
29. Abdi-Jalebi, M.; Andaji-Garmaroudi, Z.; Cacovich, S.; Stavrakas, C.; Philippe, B.; Richter, J. M.; Alsari, M.; Booker, E. P.; Hutter, E. M.; Pearson, A. J.; Lilliu, S.; Savenije, T. J.; Rensmo, H.; Divitini, G.; Ducati, C.; Friend, R. H.; Stranks, S. D., Maximizing and Stabilizing Luminescence from Halide Perovskites with Potassium Passivation. *Nature* **2018,** *555*, 497.
30. Saliba, M.; Matsui, T.; Seo, J. Y.; Domanski, K.; Correa-Baena, J. P.; Nazeeruddin, M. K.; Zakeeruddin, S. M.; Tress, W.; Abate, A.; Hagfeldt, A.; Gratzel, M., Cesium-Containing Triple Cation Perovskite Solar Cells: Improved Stability, Reproducibility and High Efficiency. *Energy & Environmental Science* **2016,** *9* (6), 1989-1997.
31. Stolterfoht, M.; Wolff, C. M.; Marquez, J. A.; Zhang, S.; Hages, C. J.; Rothhardt, D.; Albrecht, S.; Burn, P. L.; Meredith, P.; Unold, T.; Neher, D., Visualization and Suppression of Interfacial Recombination for High-Efficiency Large-Area Pin Perovskite Solar Cells. *Nature Energy* **2018**.
32. Staub, F.; Hempel, H.; Hebig, J. C.; Mock, J.; Paetzold, U. W.; Rau, U.; Unold, T.; Kirchartz, T., Beyond Bulk Lifetimes: Insights into Lead Halide Perovskite Films from Time-Resolved Photoluminescence. *Physical Review Applied* **2016,** *6* (4), 044017.
33. Krogmeier, B.; Staub, F.; Grabowski, D.; Rau, U.; Kirchartz, T., Quantitative Analysis of the Transient Photoluminescence of Ch3nh3pbi3/Pc61bm Heterojunctions by Numerical Simulations. *Sustainable Energy & Fuels* **2018,** *2*, 1027-1034.
34. Hutter, E. M.; Hofman, J. J.; Petrus, M. L.; Moes, M.; Abellón, R. D.; Docampo, P.; Savenije, T. J., Charge Transfer from Methylammonium Lead Iodide Perovskite to Organic Transport Materials: Efficiencies, Transfer Rates, and Interfacial Recombination. *Advanced Energy Materials* **2017,** *7* (13), 1602349.
35. Abebe, M. G.; Abass, A.; Gomard, G.; Zschiedrich, L.; Lemmer, U.; Richards, B. S.; Rockstuhl, C.; Paetzold, U. W., Rigorous Wave-Optical Treatment of Photon Recycling in Thermodynamics of Photovoltaics: Perovskite Thin-Film Solar Cells. *Physical Review B* **2018,** *98* (7), 075141.
36. Kirchartz, T.; Staub, F.; Rau, U., Impact of Photon Recycling on the Open-Circuit Voltage of Metal Halide Perovskite Solar Cells. In *ACS Energy Letters*, American Chemical Society: 2016; Vol. 1, pp 731-739.
37. Pazos-Outon, L. M.; Xiao, T. P.; Yablonovitch, E., Fundamental Efficiency Limit of Lead Iodide Perovskite Solar Cells. In *The Journal of Physical Chemistry Letters*, American Chemical Society: 2018; Vol. 9, pp 1703-1711.
38. Miller, O. D.; Yablonovitch, E.; Kurtz, S. R., Strong Internal and External Luminescence as Solar Cells Approach the Shockley–Queisser Limit. *IEEE Journal of Photovoltaics* **2012,** *2* (3), 303-311.